Chapter 6

Engineered Ni-Fe Prussian-blue-analogue nanocubes and their conversion into nano cage and mixed oxide for oxygen evolution reaction (OER)

6.1 Introduction

Swift in the population encourages the speediness of global industrialization development and in this scenario, the demand for sustainable and green energy has become critical. Apporoxmetly 80% of the energy is produced from fossil fuels (coal, petroleum), and we are much dependent on these energy sources for our usage. These are non-renewable energy sources with inadequate reserves, and their combustion generates harmful by-products, such as greenhouse gases which affect the environment very severely [204, 7]. This manifests the substitution of non-renewable energy sources with renewable sources, and researchers are continuously working on technologies which can convert and store different types of green energy. To apply green energy, it is imperative to develop efficient energy conversion systems [237]. Water-splitting, fuel cells and rechargeable metal-air batteries are the efficient electrochemical methods which are gaining more attention from the research community due to their feasible excellent performance in energy conversion and storage applications [238]. However, in the development of these methods, HER (hydrogen evolution reaction), OER (oxygen evolution reaction) and ORR (oxygen reduction reaction) act as the obstacle due to which harsh conditions are employed to overcome the high kinetic barrier of these reactions [239, 88, 177]. Thus, for the major benefits of these devices, study and investigation of suitable electrocatalysts are highly desirable [240].

OER reaction in water-splitting is a very important reaction for producing molecular oxygen (O_2). Oxygen is vital for living, and it has become an essential component in various industries. In the energy sector, molecular oxygen is the most widely used oxidant that accepts electrons during fuel combustion and makes chemical bonds to liberate

energy further. The industrial production approach to gaining high-concentration oxygen mainly depends on separation or purifying air, but such methods are very complicated and demand a high input of energy which hinders the goal of achieving sustainability [241]. Therefore, hastening the development of OER is crucial, and it is considered one of the most complicated processes due to its high-overpotential and low current density. It is a very sluggish reaction and hence needs a high overpotential. In both acidic and basic mediums, it is a four-protons and four electrons coupled reaction ($4OH^- \rightarrow 2H_2O + O_2 + 4e^-$ in base and $2H_2O \rightarrow 4H^+ + O_2 + 4e^-$ in acid) [7, 163].

Noble transition metal-based compounds like RuO_2, IrO_2 and Rh-Pt make up the majority of the OER catalysts that are widely used, but their scarcity and high cost prevent their widespread commercialization. To overcome the kinetic barrier and increase the reaction rates, it is necessary to build innovative catalysts with sustainability.

In the realm of energy conversion systems, Prussian blue (PB) and Prussian blue analogues (PBAs) are becoming more and more desirable materials. They are eye-catching materials for applications in variety of sectors, including sensors [95], catalysis [242], energy storage and energy conversion [243] and others due to their open-framework structure, and variable composition of earth-abundant elements. By substituting the Fe species in the PB $\{Fe_4[Fe(CN)_6]_3\}$ with transition metals such Ni, Co, and Mn, plenty of PBAs be generated with the formula of $A_xM_y[M'(CN)_6].xH_2O$ (where A represents an alkali metal ion, and M and M' are transition metal elements). Due to their varied transition metals and 3D structures, they are considered a family of metal-organic frameworks (MOFs). PBAs show promising applications in water-splitting due to their easy preparation, low-cost, tuneable compositions and environmentally friendly [244]. These compounds act as hopeful precursors and templates to obtain the different

nanostructures and compounds [98, 107] which indeed offer a new layout of the design of the green OER catalysts.

Herein, we report the synthesis of novel NiFe-Prussian blue analogue nanocube (NiFe-PBA-NC) and further their conversion into nanocages (NiFe-PBA-NG) and NiFe-mixed oxide. Firstly, nanocubes are synthesised by a precipitation method and then etched with an ammonia solution to obtain the nanocages. A control etching process is developed in which etching occurs preferentially on the corners constructing the hollow cubes. On annealing in air, the NiFe-PBA nanocubes are transformed into the NiFe-mixed oxides which are porous cubes. XRD refinement, FT-IR, XPS and FE-SEM well-confirmed the conversion of the cube to cage and oxide. Then, these materials are employed for OER analysis in which oxide show enhanced performance.

6.2 Results and discussion

6.2.1 Structual analysis using X-ray diffractometer

We have used the XRD technique to determine the composition, average crystallite size, and phase purity of the as-prepared nanocubes, and nanocages and then, verify the porous structure formation after the annealing process. As shown in Figure 6.1(a), all the diffraction peaks validate the formation of a mixed phase cubic structure of $Ni_3[Fe(CN)_6]_2(H_2O)$ and $Ni_2Fe(CN)_6$ having the space groups ‘F -4 3 m’ and ‘F m 3 m’, respectively. While the nanocages in Figure 6.1(b) are found to be pure $Ni_2Fe(CN)_6$ cubic structure (JCPDS No. 01-075-0037) with ‘F -4 3 m’ space group. After annealing at 350 °C, all the nanocubes rigorously transformed into a porous structure of cubic $Ni_{1.43}Fe_{1.7}O_4$ (JCPDS No. 01-080-0072). As shown in [Figure 6.1(c)], as-prepared porous nanocubes did not reveal any peaks other than pure cubic phase belonging to the space group ‘F d 3 m’ and space group no. 227. During cage formation, controlled etching through ammonia solution causes the removal of only the hydrated nickel iron (III)

cyanide from the nanocubes and, it is further validated through FT-IR (Figure 6.2). To confirm the cubic phase of all the nanoparticles we performed XRD profile matching & integrated intensity refinement using FullProf.2k software. As the simulated patterns matched very well with the XRD patterns, the cubic phase formation in the as-prepared nanomaterials is confirmed. All the structural information like lattice parameters, lattice volumes calculated from the Le Bail fitting are summarized in Table 6.1. As the formation of porous nanocubes introduces amorphousness in the structure, XRD peaks get broadened.

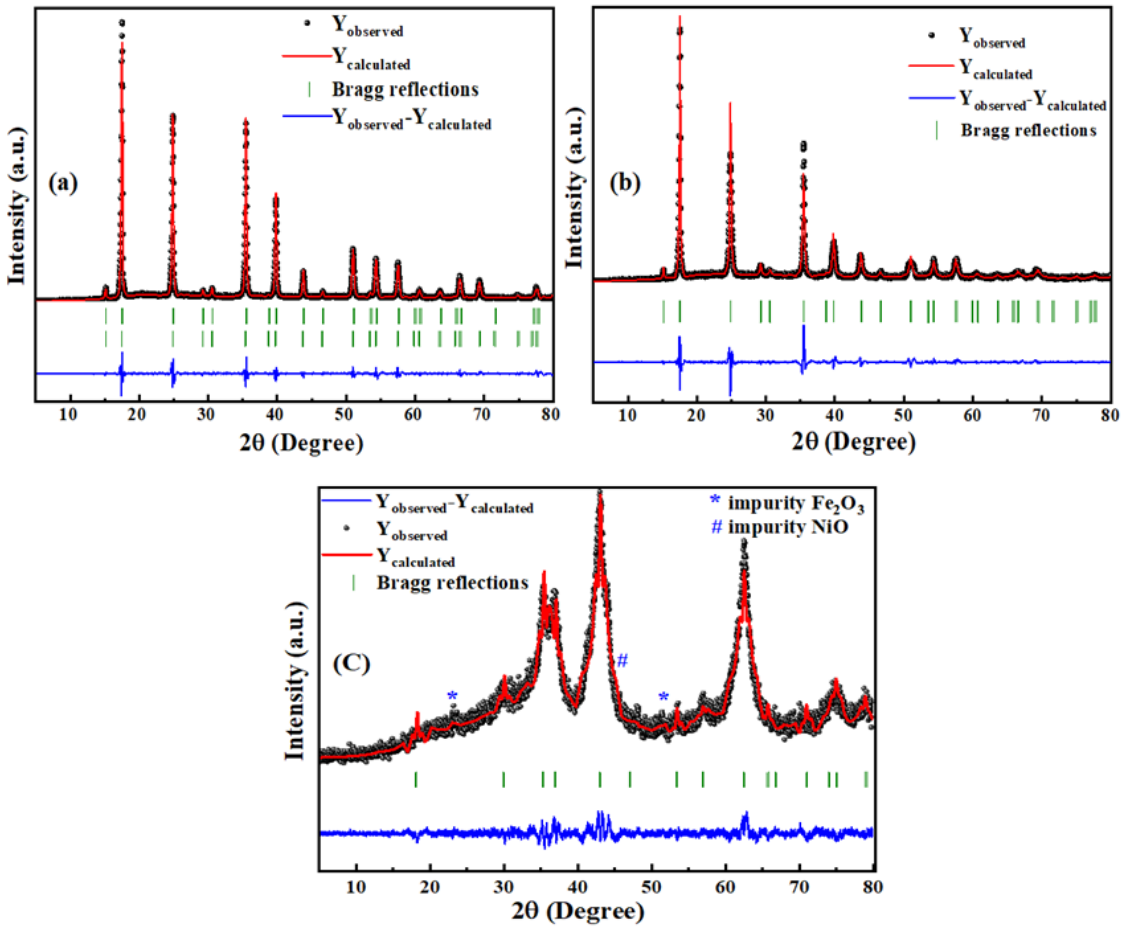

Figure 6.1 Le Bail Profile Matching & Integrated Intensity Refinement of the XRD patterns corresponding to (a) NiFe-PBA-NC, (b) NiFe-PBA-NG and (c) NiFe oxide.

Now, to calculate the average size of crystallites (*D*) that diffract coherently, we have used the Debye-Scherrer formula (Eq.2.5),

$$D = \frac{k\lambda}{\beta Cos\theta}$$

Where λ denotes the wavelength of the X-ray (1.54 Å) used, β is the integrated peak width at half maxima, and k is the constant that depends on the particle shape, often taken as 0.89 [245].

The average crystallite size of the as-prepared nickel iron cyanide nanocubes is found to be 52.32 nm which is the highest among these three nanoparticles, and then it gets reduced after both the ammonia and heat treatment. From our understanding, this is because, both the porosification treatment, ammonia etching and -CN bond breaking through annealing reduce the coherence between domains.

Table 6.1: Structural parameters for materials from the XRD refinement.

Structural parameters	**NiFe-PBA-NC**		**NiFe-PBA-NG $Ni_2Fe(CN)_6$**	**NiFe mixed oxide $Ni_{1.43}Fe_{1.7}O_4$**
	Phase 1 $Ni_3[Fe(CN)_6]_2(H_2O)$	**Phase 2 $Ni_2Fe(CN)_6$**		
a (Å); b (Å); c (Å)	10.11705	10.14359	10.13147	8.397669
Volume ($Å^3$)	1035.5	1043.7	1039.961	592.2
α(°); β(°); γ(°)	90.0	90.0	90.0	90.0
χ^2	2.42		3.74	2.26
Average crystallite size (nm)	52.32		34.61	6.54

6.2.2 FT-IR analysis and etching mechanism

Fourier transform infrared (FT-IR) spectroscopy has been used to examine the structure of synthesized NiFe-PBA-NC, NiFe-PBA-NG and NiFe oxide. Figure 6.2 shows the spectrum of NiFe-PBA-NC, NiFe-PBA-NG and NiFe oxide. Both NiFe-PBA-NC and NiFe-PBA-NG exhibit the distinctive vibrations of Ni(II)-N≡C-Fe(II) and Ni(II)-N≡C-Fe(III) species at 2092 and 2164 cm^{-1}, indicating the nature of C≡N bond in nanocube and nanocage, respectively. While these peaks are absent in NiFe oxide, confirms the

decomposition of -CN (-C≡N) groups from the nanocubes as evidenced by the amorphous XRD nature [90, 97]. NiFe-PBA-NC and Ni-Fe-PBA-NG both show O-H stretching vibration at 3418 cm^{-1} while in the NiFe oxide, it is present at 3437 cm^{-1}.

H-O-H bending in all three compounds is present at 1608 cm^{-1}. Instead of this, NiFe oxide shows peaks at 1380 and 830 cm^{-1} due to symmetrical stretching vibration of atmospheric CO_2 (O-C=O) and Ni-O, Fe-O bonds, respectively. In the process of obtaining nanocage from nanocube, when NiFe-PBA-NC is etched with ammonia solution, ammonia etching mostly occurs at the Ni(II)-N≡C-Fe(III) rather than Ni(II)-N≡C-Fe(II) because Fe^{III} species have a larger affinity for the cyanide group (CN) than Fe^{II} species do. This shows that the N atom's ability to donate electrons is less in the -N≡C-Fe(III) species than it is in the -N≡C-Fe(II) species. As a result, the bond formed by Ni^{II} and -N≡C-Fe(III) should be weaker and more easily broken than the one created by Ni^{II} and -N≡C-Fe(II). As found in FTIR spectra, the intensity ratio corresponding to 2092 cm^{-1} and 2164 cm^{-1} enhances ~18 times while transforming cubes to cages. The following reactions are probably involved in this etching process:

$$Ni_3^{II}[Fe^{III}(CN)_6]_2 + 18\,NH_3 \rightarrow 3[Ni(NH_3)_6]^{2+} + 2[\mathrm{Fe}(CN)_6]^{3-} \quad \text{(Eq. 6.2)}$$

$$6[\mathrm{Fe(CN)_6}]^{3-} + 8NH_3 \rightarrow 6[Fe(CN)_6]^{4-} + N_2 \uparrow + 6NH_4{}^{+} \quad \text{(Eq. 6.3)}$$

By coordinating with ammonia in a ligand exchange reaction, the aforementioned equations suggest that Ni^{2+} from Ni(II)-N≡C-Fe(III) sites can be stabilized (Eq. 6.2). Moreover, the etching procedure could also entail a redox reaction can (Eq. 6.3). A peak is seen at 1415 cm^{-1} in the spectrum of NiFe-PBA-NG due to NH vibration for NH^{4+}, further supporting the existence of the redox process during the ammonia treatment.

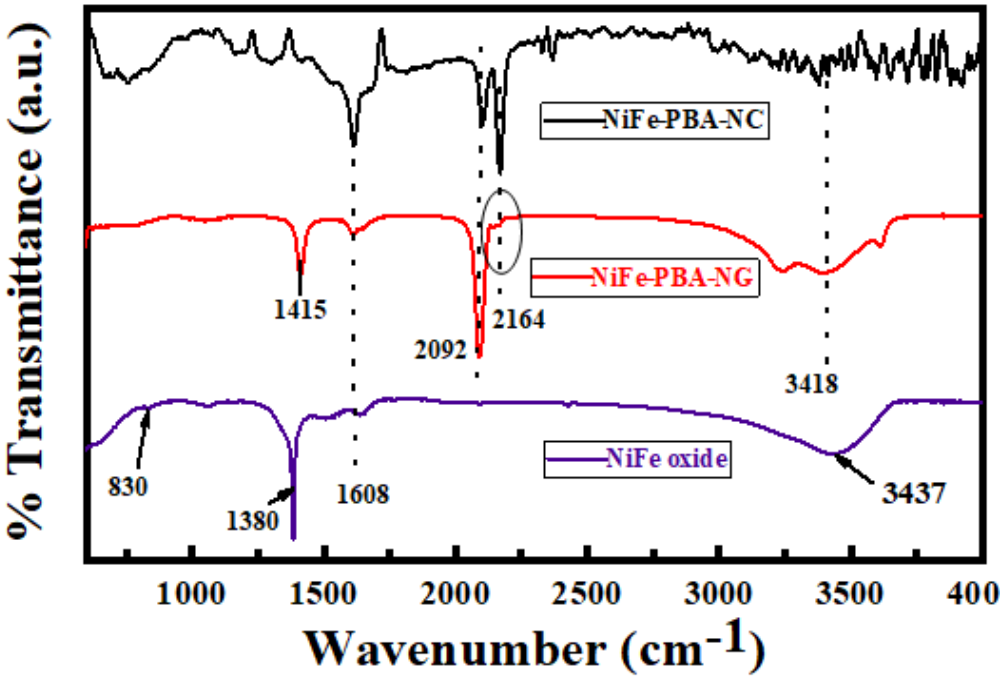

Figure 6.2 FTIR spectrum of NiFe-PBA-NC, NiFe-PBA-NG and NiFe oxide.

6.2.3 XPS study

To study the chemical composition present in all the samples, XPS spectra are deconvoluted and described thoroughly. Figure 6.3 shows the XPS of NiFe-PBA-NC. Ni, Fe, C, N and O elements are confirmed to be present in nanocubes by full scan survey spectrum [Figure 6.3(a)]. Spectrum of Ni 2p is deconvoluted into four peaks corresponding to Ni $2p_{3/2}$ (856.2 eV), Ni $2p_{1/2}$ (873.8 eV) and their satellite peaks at 863.1 eV and 880.7 eV, respectively, confirming the presence of Ni^{2+} in the nanocubes. The spectrum of Fe 2p is fitted by mainly two peaks Fe $2p_{3/2}$ and Fe $2p_{1/2}$ and their satellites peaks. Fe $2p_{3/2}$ and Fe $2p_{1/2}$ are further deconvoluted into three peaks each. Binding energies at 709.7 and 723.4 eV due to Fe^{3+} $2p_{3/2}$ and Fe^{3+} $2p_{1/2}$ of $[Fe^{3+}(CN)_6]$ in the PBA framework [90] whereas the peaks at 711.2 eV and 725.8 eV due to presence of Fe(OH)O (because of coordinated water molecules in framework) in $2p_{3/2}$ and $2p_{1/2}$, respectively. Peaks at 708.2 eV and 721.2 eV correspond to Fe^{2+} $2p_{3/2}$ and Fe^{2+} $2p_{1/2}$ of $[Fe^{2+}(CN)_6]$ in PBA, respectively while binding energies at around 713.6 eV and 737.3 eV belongs to

satellite peaks. Both divalent and trivalent Fe coexist in NiFe-PBA nanocube, according to XPS observations, which are also consistent with our FTIR findings. In the high-resolution spectrum of C 1s [Figure 6.3(d)] characteristic peak of C≡N emerges at 284.2 eV, while other peaks at binding energies 284.2, 285.1 and 286.3 eV correspond to the C=C (C-C), C-O and N-C=O bonds, respectively. N 1s spectrum is fitted into four peaks shown in [Figure 6.3(e)] in which binding energy at 397.8 eV is ascribed to the cyanide group present in the PBA lattice whereas peaks at 398.2, 398.6 and 399.8 eV can be allocated for pyridine N, graphitic N and oxide N [246]. In the spectrum of O 1s, peaks originated at 532.4, 533.0 and 533.5 due to C=O, C-O and C-OH, respectively [247].

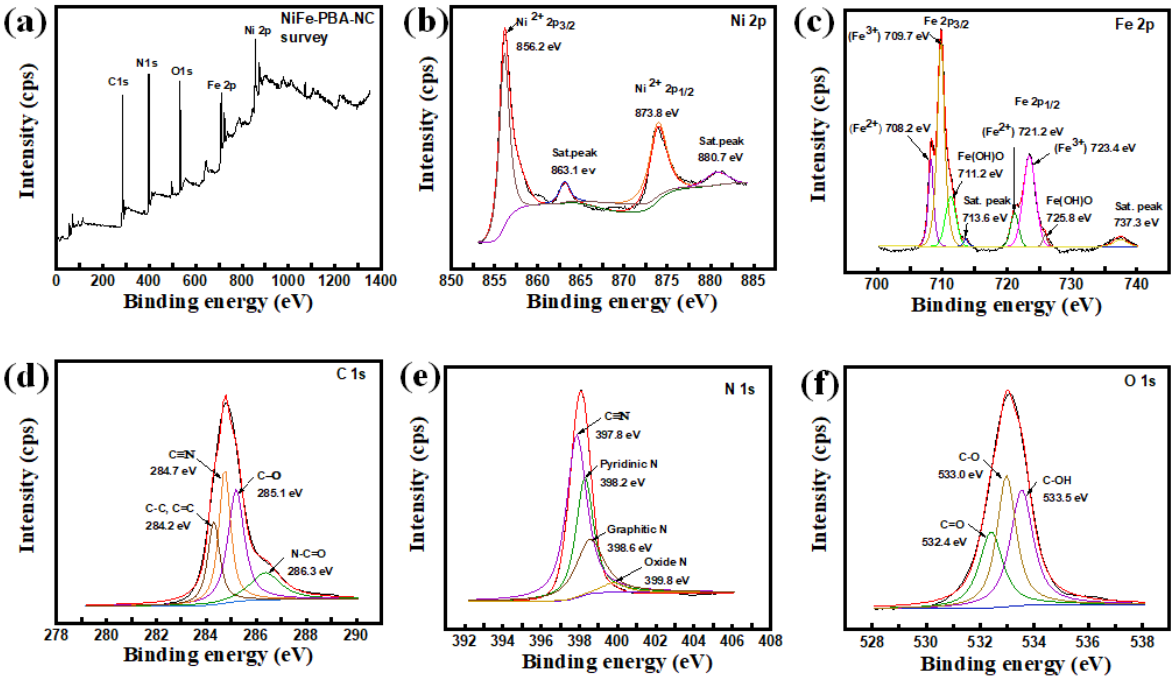

Figure 6.3 XPS for NiFe-PBA-NC corresponding to (a) survey, (b) Ni 2p, (c) Fe 2p, (d) C 1s, (e) N 1s and (f) O 1s.

The chemical environment and composition of NiFe-PBA-NG are the same as those of NiFe-PBA-NC, according to an XPS analysis [Figure 6.4(a)]. The existence of Ni^{2+} is confirmed by Ni 2p spectrum, which displays two peaks at 856.6 eV (Ni $2p_{3/2}$) and 874.3 eV (Ni $2p_{1/2}$) along with their satellite peaks at 862.9 and 880.5 eV as in the NiFe-PBA-NC. In the case of the Fe 2p spectrum, $2p_{3/2}$ and $2p_{1/2}$ shows deconvoluted peaks for Fe^{2+}

and Fe^{3+}. The intensity of Fe^{3+} peaks is very less than that to Fe^{2+} peaks [Figure 6.4(c)] indicating that the most of Fe^{3+} species being leached out during the etching process of nanocubes while Fe^{2+} species remain unchanged. This outcome is also supported by XRD and FTIR results (*vide supra*), validating our controlled etching mechanism. Spectra of C1s, N 1s and O 1s have similar peaks as in nanocubes.

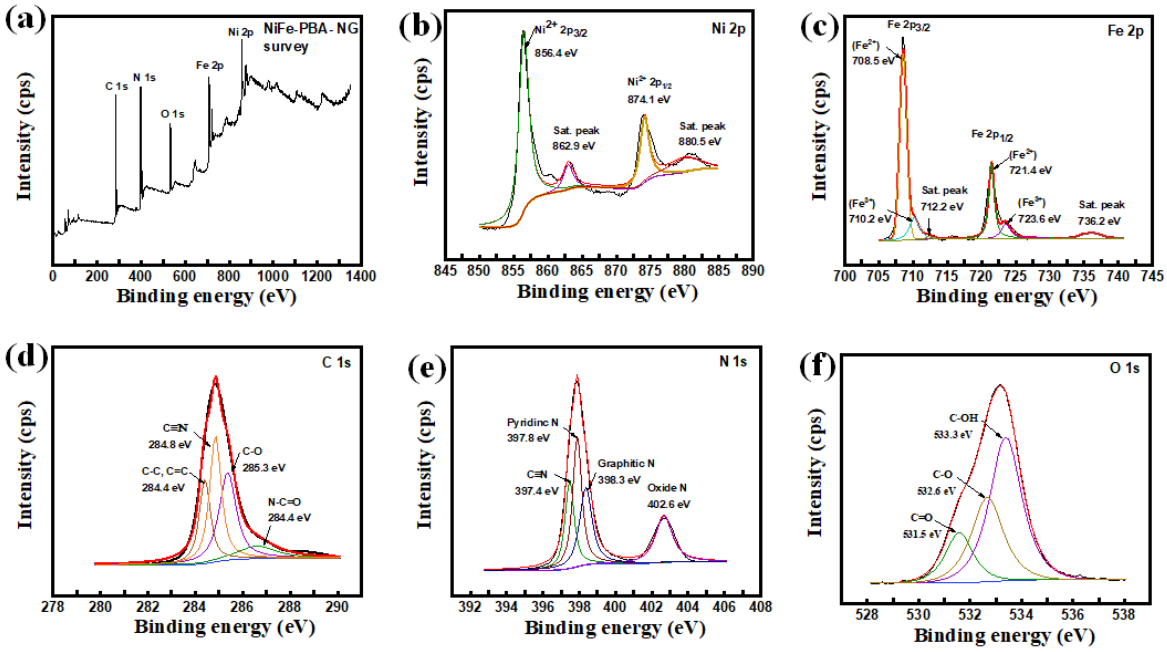

Figure 6.4 XPS for NiFe-PBA-NG corresponding to (a) survey, (b) Ni 2p, (c) Fe 2p, (d) C 1s, (e) N 1s and (f) O 1s.

Full survey scan [Figure 6.5(a)] shows the elements Ni, Fe and O present in the oxide cube. Spectrum of Ni 2p [Figure 6.5(b)] shows two main peaks Ni $2p_{3/2}$ and Ni $2p_{1/2}$ and their satellite peaks. In $2p_{3/2}$, binding energy at 854 eV indicate the Ni^{2+} in octahedral site (Oh) [7] whereas peak at 855.4 eV shows the presence of NiO formed during heat treatment of NiFe-PBA-NC. Similarly, for $2p_{1/2}$, binding energy at 871.4 eV (Ni^{2+} in Oh) and 872.9 eV (NiO) observed. Satellite peaks at around 861 and 862.5 eV for $2p_{3/2}$ and for $2p_{1/2}$ observed at 878.6 and 880.7 eV for Ni^{2+} in Oh and NiO, respectively [248]. In the case of Fe 2p spectrum, two peaks are found Fe $2p_{3/2}$ and Fe $2p_{1/2}$ [Figure 6.5(c)]. In the case of Fe $2p_{3/2}$, binding energies at 710.3 and 712.4 eV indicate that the octahedral

and tetrahedral sites, respectively are occupied and the single satellite peak observed at 718.89 eV supports the existence of Fe^{3+}. Fe $2p_{1/2}$ and satellite peak positioned at 724.4 and 732.7 eV, respectively which further reconfirm the Fe^{3+} in oxide cube [7]. O 1s spectrum [Figure 6.5(d)] shows two peaks at 529.4 and 532 eV in which binding energy at 529.4 eV due to Ni(II)−O and Fe(III)−O bonds whereas peak at 532 eV shows the chemisorbed oxygen in the material.

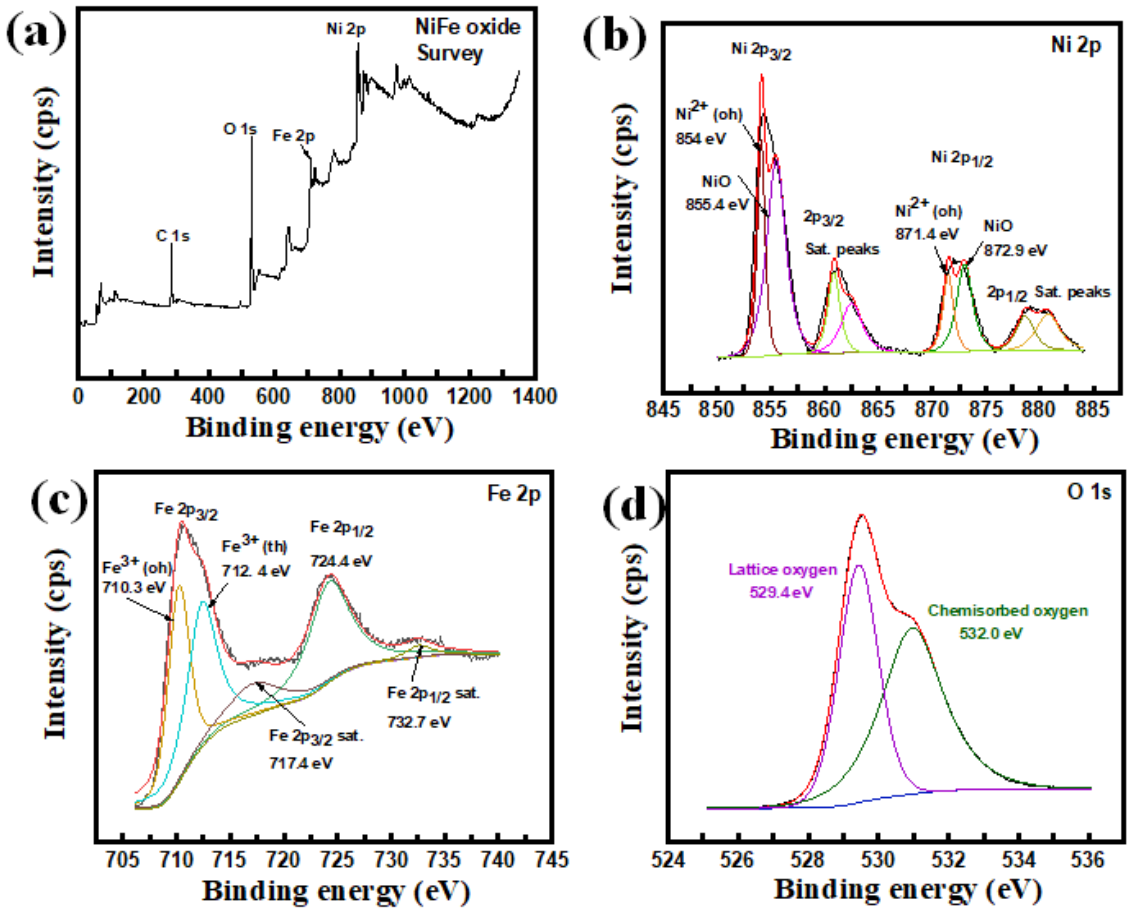

Figure 6.5 XPS for NiFe oxide corresponding to (a) survey, (b) Ni 2p, (c) Fe 2p and (d) O 1s.

6.2.4 Thermogravimetric analysis (TGA)

Thermogravimetric measurements are carried out from room temperature to 550 °C to examine the thermal stability and water contents of the NiFe-PBA-NC. Between 35 °C and 550 °C, numerous weight loss processes for NiFe-PBA-NC may be seen in Figure

6.6. Prior to 200 °C, weight loss often results from the physical loss of adsorbed water, whereas weight loss between 200 °C and 350 °C is caused by volatilization of coordinated water molecules. There has been a 20.17% overall water loss [246]. After that, a significant weight loss (23.69%) is observed over a temperature of 350 °C, which indicates the decomposition of -C≡N bond in the PBA framework.

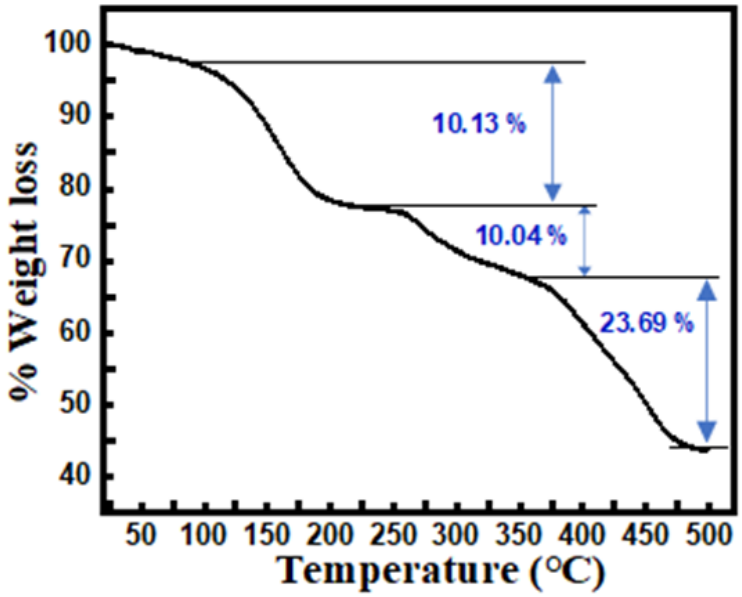

Figure 6.6 TGA of NiFe-PBA-NC.

6.2.5 Morphological study and BET

Surface morphology (Figure 6.7) and particle size distribution corresponding to all three materials are being analysed through HR-SEM images. NiFe-PBA-NC at different magnifications [Figure 6.7(a, a')] reveals a perfect cubical morphology having very smooth surfaces and almost identical size. As shown in the size distribution curve in the inset of the image, the average size of cubes is ~200 nm. When solid nanocubes are treated with ammonia solution cage-like morphology is formed [Figure 6.7(b, b')]. The nanocages also have a cubic structure but with etched edges. The degree of etching probability is the highest at all eight corners, then edges and lastly at the flat planes owing to the relative surface energy as well as the exposed surface area to interact with. Cavities are observed at the corners of the nanocubes, suggesting a more open structure of the

nanocages. For direct visualization of the internal structure, we take HR-SEM images of broken intermediates [Figure 6.8(e)]. Whereas, in the process of annealing of nanocubes for 3 hours at 350 °C in the presence of O_2 atmosphere, decomposition of the CN bonds from the PBA framework of nanocubes yields a porous morphology due to CO_x, NO_x gas emission. Figure 6.7(c, c') shows the porous oxide also retains the cubic shape with average particle size of 116 nm.

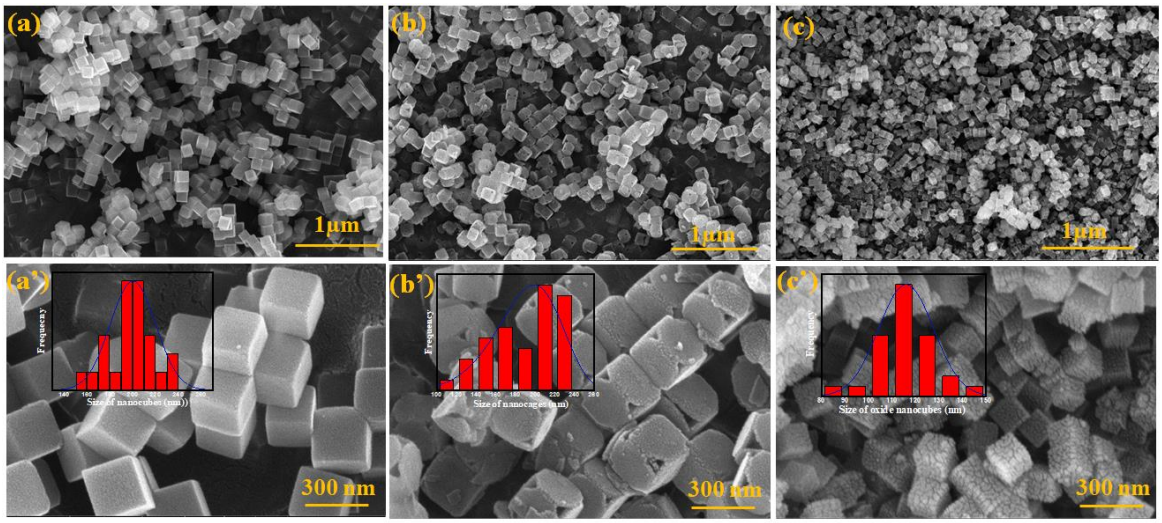

Figure 6.7 HR-SEM image of (a, a') NiFe-PBA-NC, (b, b') NiFe-PBA-NG and (c, c') NiFe oxide.

To determine the porosity of as-synthesized materials BET and BJH methods are employed. For NiFe-PBA-NC, NiFe-PBA-NG and NiFe oxide, Figure 6.9 presents the N_2 adsorption-desorption isotherm and corresponding pore size distribution from BJH plots. Isotherm plots are similar to Type IV and correlate well with earlier results [7]. Surface area, pore volume and pore diameter of each material is given in Table 6.2.

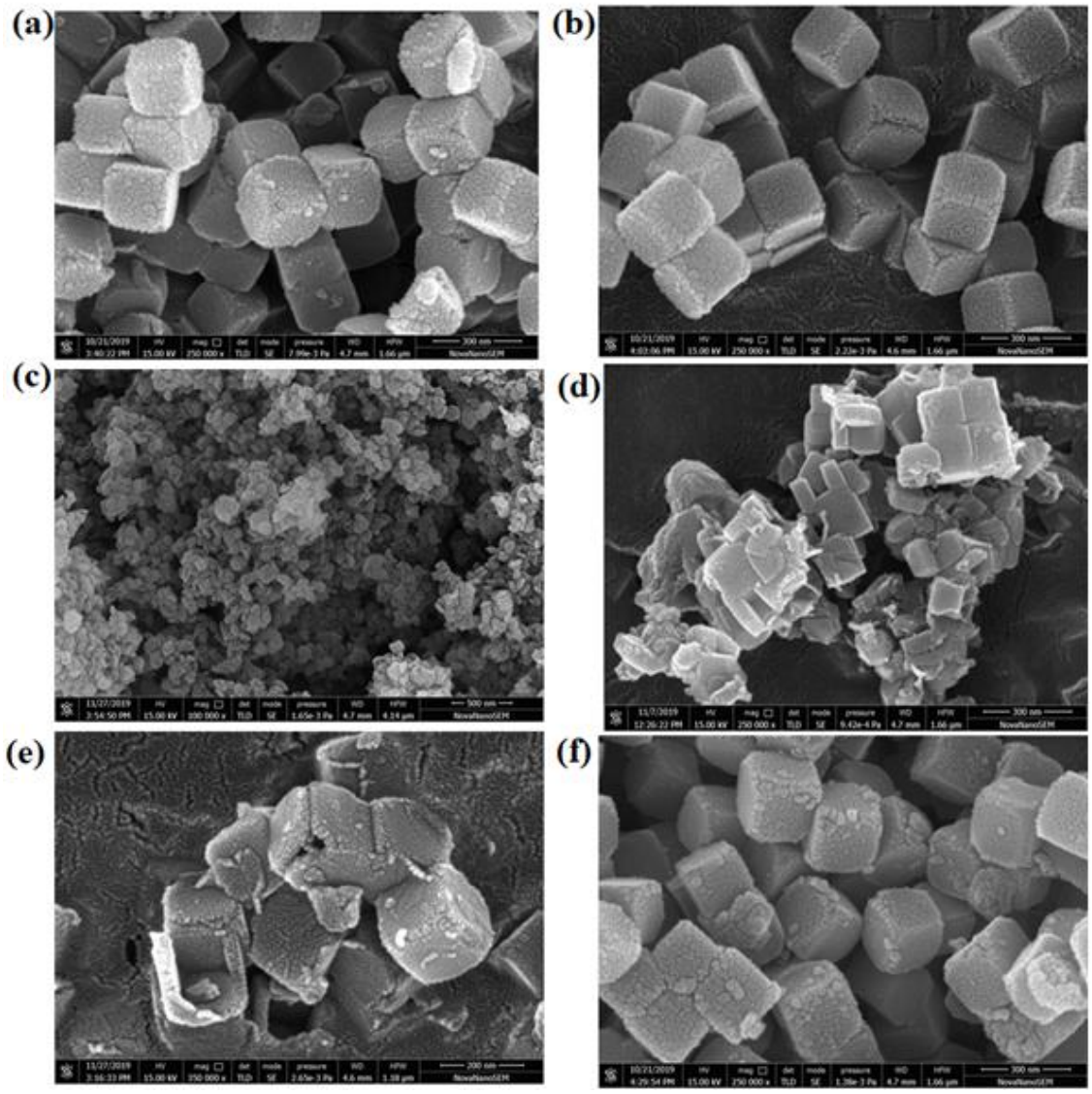

Figure 6.8 Optimization of ammonia solution and time (a) 500 µL, 1 hour; (b) 1.3 mL, 1 hour; (c) 3.5 mL, 1hour; (d) 5 mL, 2 hour; (e) 2.6 mL , 5 hour; (f) 500 µL , 15 hour for nanocage formation from nanocubes.

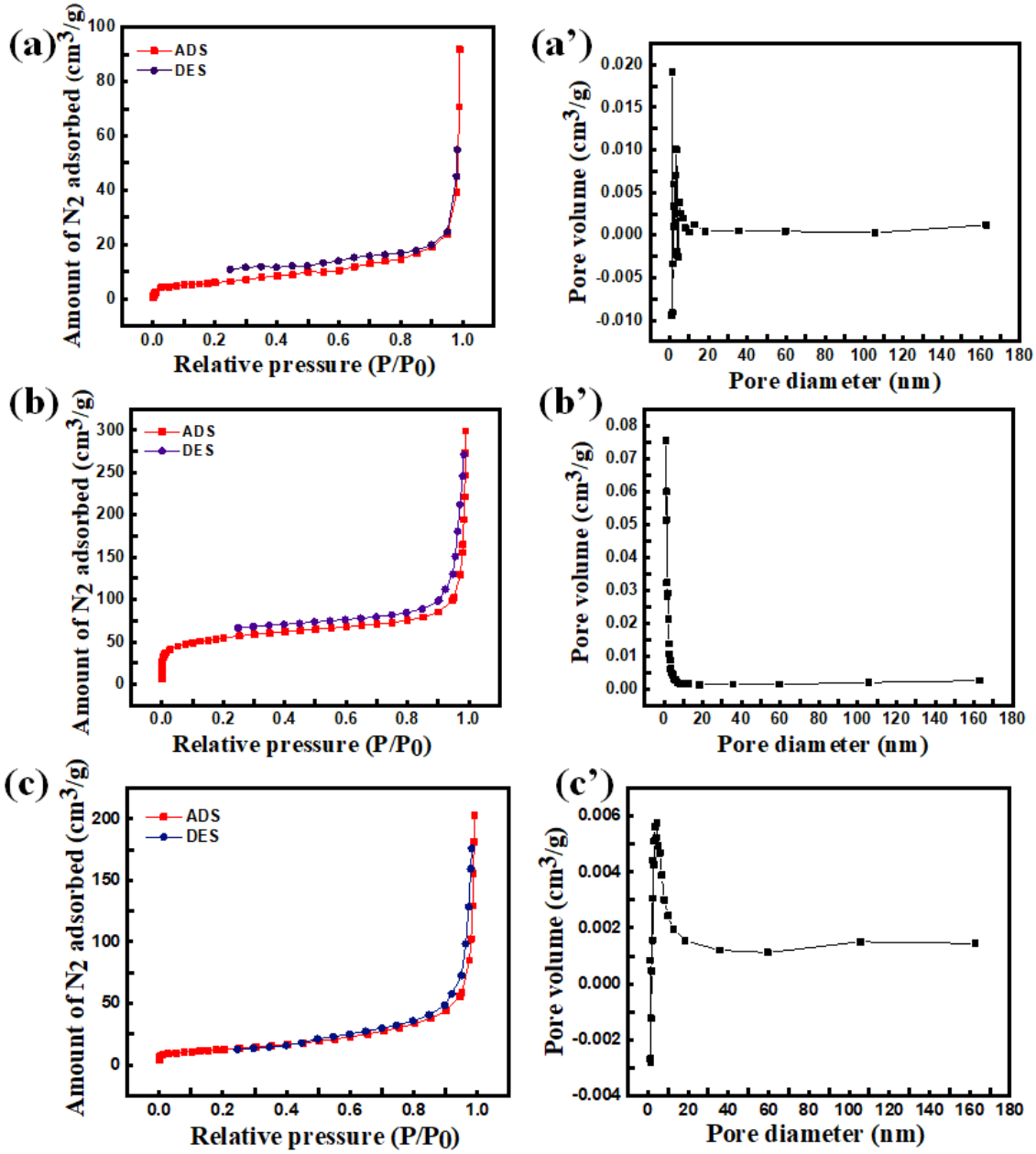

Figure 6.9 N_2 adsorption-desorption isotherms of (a) NiFe-PBA-NC, (b) NiFe-PBA-NG, (c) NiFe oxide and the corresponding NL-DFT pore size distribution (a') NiFe-PBA-NC, (b') NiFe-PBA-NG and (c') NiFe oxide.

Table 6.2 BET surface area and other parameters of the materials.

Materials	BET surface area ($m^2 g^{-1}$)	Pore Volume ($cm^3 g^{-1}$)	Pore diameter (nm)
NiFe-PBA-NC	21.6	0.1228	22.8
NiFe-PBA-NG	184	0.4626	10.0
NiFe oxide	44.5	0.2965	26.7

6.2.6 Oxygen evolution reaction (OER) study

The OER performance of all as-synthesized catalysts used for modification of commercial GCE was studied and compared by LSV and EIS. As depicted from Figure 6.10(a), nanocubes to nanocages catalytic current increases. The increase in the current is due to more surface area and opens up of pores in nanocages. By etching process cavities are generated at corners [Figure 6.7(b, b)] which enhances its surface area and opens the pores of nanocubes. NiFe oxide has higher catalytic activity than nanocubes and nanocages. The catalytic current is also larger than the state of the art catalyst RuO_2. The variation in the catalytic performance is due to different oxygen vacancy. From XPS measurement oxygen atomic weight percentage is measured and it is found to 16.68, 13.15 and 42.92 for nanocubes, nanocages and oxide. Although nanocages has higher surface area than oxide, but the oxygen vacancy is lower than oxide. Tafel slope is an inherent property of the catalyst which determines the electrocatalytic activity of the

catalyst. For the comparison of the performance of the as-synthesized catalysts, we have calculated Tafel slopes fitting well with the Tafel equation 1.40 for NiFe-PBA-NC, NiFe-PBA-NG and NiFe mixed oxide and compare with RuO_2. It was found that NiFe oxide has lowest tafel slope (47.4 $mVdec^{-1}$) among nanocubes and nanocages which is also confirmed by the EIS plot [Figure 6.10(c)], having lower R_{ct}.

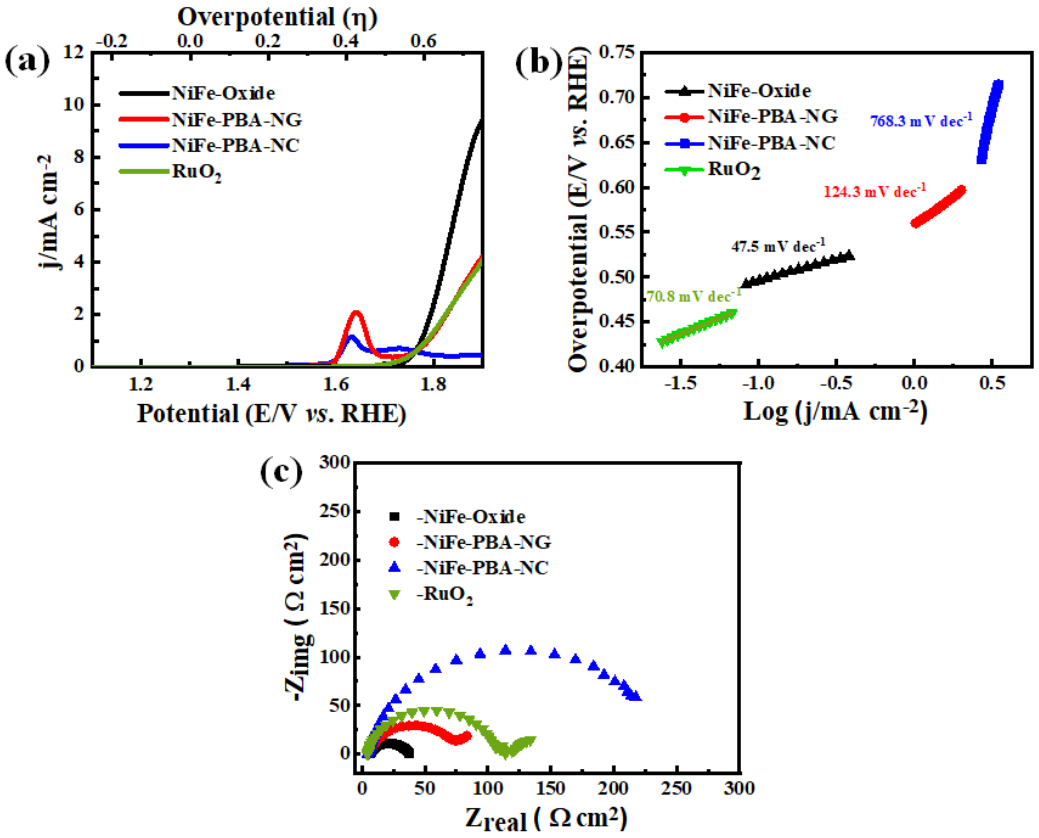

Figure 6.10 (a) LSV, (b) Tafel slopes, (c) Nyquist plots of NiFe-PBA-NC, NiFe-PBA-NG, NiFe oxide and RuO_2 at scan rates of 5 mVs^{-1} in 0.1 M KOH.

6.3 Conclusions

In summary, this work demonstrates the synthesis of a novel Ni-Fe Prussian blue analogue nanocube (Ni-Fe PBA NC) as an electrocatalyst for OER. Further, using nanocubes as templates, different two nanostructures are derived using different conditions. The control etching process generates the nanocage (NiFe-PBA-NG), in which materials are leached out from the corners, and the structure becomes hollow. At the same time, the annealing process creates NiFe-oxide, a porous cube, due to the

decomposition of cyanide bonds. Despite the different conditions employed, both nanostructures retain their cubic morphology with different chemical compositions. In nanocubes, two phases are found corresponding to Fe^{2+} and Fe^{3+}, but in nanocage, only Fe^{2+} remains because Fe^{3+} reacts with the ammonia solution (reactivity; $Fe^{3+} > Fe^{2+}$) and in the presence of air, at 350 ℃, all Fe^{2+} are oxidised into Fe^{3+}, showing only Fe^{3+} in the oxide. Although the nanocage has a higher surface area than the NiFe-oxide but it offers lesser OER performance because the Fe^{3+} species in the nanocage is leached out.